Coherent spontaneous emission of light by thermal sources

F. Marquier, K. Joulain, J.-P. Mulet, R. Carminati, and J.-J. Greffet
Laboratoire d'Énergétique Moléculaire et Macroscopique; Combustion, École Centrale Paris, Centre National de la Recherche Scientifique, Grande Voie des Vignes, 92295 Châtenay-Malabry Cedex, France

Y. Chen
Laboratoire de Photonique et Nanostructures, Centre National de la Recherche Scientifique, 91460 Marcoussis, France
(Received 21 November 2003; published 14 April 2004)

The emission of light by a material at temperature T has been shown recently to be coherent in the near field. These properties were attributed to the thermal excitation of surface polaritons. We review the origin of this phenomenon. We analyze the influence of the microstructure and temperature on the coherence properties and show how to engineer thermoradiative properties of surfaces. We report the design of a quasi-isotropic source and a very directional source of thermal light. We also report a measurement of the transverse coherence length of a thermal source of light.

DOI: 10.1103/PhysRevB.69.155412 PACS number(s): 73.20.Mf, 78.68.+m, 71.36.+c, 44.40.+a

I. INTRODUCTION

The tungsten filaments of light bulbs are certainly the most widely used sources of light. The microscopic mechanism of light generation is the spontaneous emission of a photon when an emitter thermally excited relaxes to a lower state. Such light sources are called thermal sources. They are usually almost isotropic sources of light with a broad spectrum. This contrasts with a laser that produces very directional and monochromatic light. The narrow spectrum is a measure of the temporal coherence of the source, whereas the directivity is a measure of its spatial transverse coherence. Recently, it has been realized[1–3] that a thermal source of light could be coherent in the near field, i.e., when analyzing the light at distances of the surface much smaller than the peak wavelength of the spectrum. Further work has led to the construction of a coherent thermal source of light.[4] It has thus been shown that a source based on spontaneous emission may produce light that is partially coherent, both spatially and temporally. In this paper, we shall report a detailed study of this type of source and discuss the role of surface waves in building coherent fields. We will report a measurement of the coherence length of the field along the source. We will also carefully study the role of the temperature on the emission. We will finally report measurements on a type of source that produces an isotropic emission of light.

The emission of light by hot bodies is usually discussed in the context of energy transfer or thermodynamics using phenomenological concepts such as absorptivity, emissivity, and specific intensity.[5,6] However, it is possible to address this problem in the framework of classical electrodynamics. This approach was first used by Lorentz[7] but, at that time, the statistical properties of the random currents were not known, so that it was impossible to obtain the Planck function following this route. This is why this type of approach has been abandoned in textbooks. Indeed, radiation in a vacuum, i.e., blackbody radiation, is usually derived using the Bose-Einstein statistics for photons. This approach can be used only if the electromagnetic states of the system are known and at thermodynamic equilibrium. Nonequilibrium phenomena such as emission by a specific material are usually described using a phenomenological theory. None of these theories allows one to derive the emitted fields starting from the basic principles of electrodynamics.

The basic idea of an electromagnetic treatment of thermal radiation is that each volume element of a body at temperature T can be viewed as a random electric dipole. Indeed, because of the random thermal motions of electrons and ions, there are random currents in the material. Therefore, each volume element can be viewed as an electric dipole that generates an electric field. Next, we have to derive the field generated by a dipole below an interface. This is a standard problem that was first solved by Sommerfeld. A detailed discussion can be found in the monograph by Banos.[8] Although the solution involves some integrals that may not be easy to evaluate analytically, the problem can be worked out numerically.[9] It is worthwhile to point out that all the optical properties of the medium and all the resonances of the interface are taken into account when computing the field emitted by a dipole below the interface (i.e., the Green tensor of the problem). Because the mean value of the current is null, the mean value of the electric field is also null. The quantity that is then needed is the correlation function of the current density which is given by the fluctuation-dissipation theorem derived in 1951.[10] The full treatment was first given by Rytov *et al.*[11] It was applied by these authors mostly to radio waves emission problems, but the framework is valid for any frequency. For instance, this approach allows one to derive rigorously the emissivity for a flat surface and thus to retrieve the usual phenomenological result. Furthermore it yields the field in the vicinity of the interface because surface modes are fully taken into account. When surface waves can exist, the field is completely dominated by these thermally excited surface waves. They produce unexpected results. First of all, the spectrum of the energy density becomes almost monochromatic.[2] Its Fourier transform yields the first order (i.e., amplitude) correlation function according to the Wiener-Khinchin theorem. It appears that the field has a long coherence time. Second, the density of energy increases by several orders of magnitude.[1,2] Third, the field can be shown to be spatially coherent over distances much larger than the wavelength along the interface.[1,3] These facts contradict the

widely accepted point of view that a thermal source of light is incoherent. All these effects cannot be detected in the far field because they are due to surface waves which decay exponentially away from the interface. Yet, roughness can couple surface waves to propagating waves, and thus transfer the coherence properties into the far field.[4] Note that we do not claim that a thermal source produces a laserlike field. First of all, the mean occupancy number of each state is still given by the Bose-Einstein law. Second, the intensity statistics are very different for a laser and a thermal source. However, surface waves do produce a significant time and spatial second order coherence of the field in the near-field. This coherence can be used to modify significantly the radiative properties of surfaces.

To proceed, one can modify the surface profile. It has been known for a long time that microroughness modifies radiative properties. In particular, the influence of a grating on the absorption properties has been studied in great detail.[12] A spectacular effect was predicted and verified experimentally[13] in 1976: ruling a shallow sinusoidal grating on a gold surface may lead to a total absorption of visible light for a particular polarization. This behavior has been associated with the resonant excitation of a surface mode: a surface plasmon polariton. Due to its resonant character, this absorption takes place for a particular angle once the frequency is fixed.

Absorption is not the only radiative property that depends on the surface profile. According to Kirchhoff's law, the emissivity of a surface is equal to the absorptivity for the same frequency, same direction, and same polarization. Its validity has been a subject of debate for some time but the question was finally settled[5] when a proof was derived from the reciprocity theorem that follows from Maxwell's equations. Based on this argument, it is thus expected to observe a manifestation of surface waves on the emission of light by surfaces. This has indeed been observed recently by Kreiter *et al.*[14] on a gold surface heated at 700 °C. Because of the range of temperature needed, it is easier to observe these effects in the infrared. Although surface plasmon polaritons may exist for highly doped semiconductors, it is easier to observe these phenomena by taking advantage of a different type of surface waves. They are called surface phonon polaritons. They can be viewed schematically as phonons in an ionic crystal. The mechanical vibration of the ions generates a charge oscillation and therefore an electromagnetic wave.

In the early 1980s, Zhizhin *et al.* studied thermal emission of materials supporting surface phonon polaritons.[15] They worked with a ZnSe crystal sample including periodic inhomogeneities on its surface. The sample was heated at 150 °C in order to excite surface waves. Coupling these waves with the periodic profile, they observed emissivity spectra in the *p* polarization changing with the direction of observation. That observation was a signature of the excitation of a surface wave. It is worth mentioning that the emission assisted by the excitation of a surface wave has been used in a different context. In the late 1980s, Gruhlke, Holland, and Hall observed the luminescence by atoms placed in a film with a grating on top of it. They observed that the presence of the grating modified significantly the emission. The interpretation is that the emission of the atoms excited a surface mode that was subsequently diffracted by the grating.[16] It is interesting to compare the two emission phenomena because they have the same basic mechanism. The spontaneous emission of light by a metallic grating can be viewed as follows: (i) nonradiative decay of a thermally excited electron or phonon into a surface phonon polariton, and (ii) diffraction of the surface phonon polariton by the grating. Other authors have used this idea more recently. Let us mention the enhanced fluorescence of emitters (Eu^{3+}) located in close proximity to a metallic grating surface[17] and the extraction of light emitted by an active source located inside a modulated structure.[18]

Later on, Hesketh and Zemel measured thermal emission at 400 °C of doped silicon gratings. They observed resonances in the emission amplitude in the *p* polarization and different spectra when varying the grating period.[19–21] As we will see, the phenomenon reported by Hesketh and Zemel was related to the presence of surface plasmon polaritons and not to organ pipe modes, as first thought. Many other authors have experimentally explored the role of texture on emissivity. We will not mention here the works done on gratings with a period larger than the wavelength so that the geometric optics apply. In 1995, Auslander and Hava studied anomalous reflectance in doped silicon lamellar gratings due to the surface profile of a grating. Yet, they worked in *s* polarization,[22] so that these effects were not related to surface wave excitation. Nevertheless they noticed in 1998 an antireflective behavior in the *p* polarization for V-grooved silicon grating with a SiO_2 mask layer.[23] Sai *et al.* also made calculations and measurements on a three-dimensional V-grooved silicon grating with an SiO_2 mask layer and interpreted their observation in terms of resonance between the field and the grating.[24] Le Gall *et al.*[25] showed that the emissivity of SiC could be increased by ruling a grating. Finally, let us mention a recent attempt to use a photonic crystal structure of tungsten to modify the radiative properties.[26]

In this paper, we will report a detailed study of the thermal emission due to the thermal excitation of surface phonon polaritons. Recent papers[1,2] have shown that the presence of surface waves on a plane interface enhance the temporal and spatial coherence close to the interface (at distances smaller than the typical wavelength given by the Wien displacement law, 10 μm at 300 K, for example). This yields insight into the mechanism of light emission. We will first review these ideas. We will then study the interplay between the disorder of the microstructure of a material and the spatial coherence of the field by comparing amorphous and crystalline silica. We will then describe an experimental setup designed to enhance the angular and spectral resolution of emission measurements. We will report a detailed experimental study of the emission of a grating. We will, in particular, examine carefully the role of temperature in the results. We will also show that it is possible to engineer the radiative properties of a surface by a proper design of the grating profile using a rigorous coupled wave analysis (RCWA) algorithm.[27] Two thermal sources have been realized. The first source radiates almost isotropically but with an emissivity enhanced by more than an order of magnitude. The second source has an

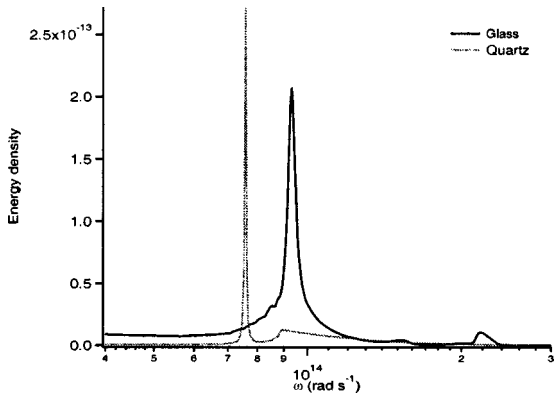

FIG. 1. Energy density above a vacuum-silica interface in the near field. Note the shift of the peak frequency depending on the microscopic structure.

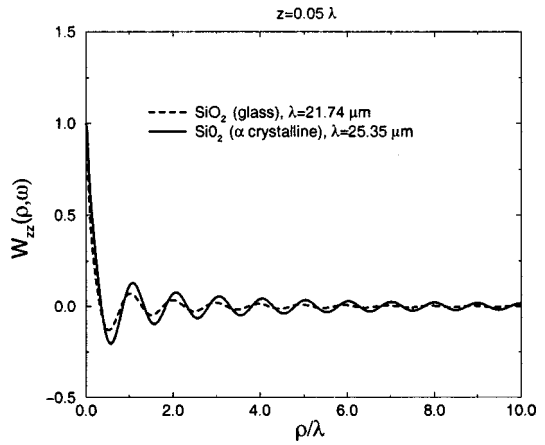

FIG. 2. Cross-spectral density of the *z* component of the electric field above a vacuum-glass interface. Note that the coherence length of the amorphous silica is smaller than for the crystalline form.

emission pattern that displays two narrow lobes like an antenna. Finally, we will show how the coherence length along the source can be recovered from our far field emission measurements and discuss qualitatively the origin of the spatial coherence.

II. COHERENCE IN THE NEAR FIELD

A. Temporal coherence in the near field

In this section we consider the emission of light by a half space containing silica, either amorphous (glass) or cristalline (quartz). The upper half space is a vacuum. We plot the density of electromagnetic energy as a function of frequency in the near field in Fig. 1. We see that the spectrum is no longer a broad spectrum with an envelope given by the Planck function; instead, the spectrum has a narrow peak. This is a signature of the temporal coherence of the electromagnetic field close to the interface. A striking property is the numerical value of the density of energy. It is roughly larger than the density in vacuum by four orders of magnitude. Similar results for SiC were first reported in Ref. 2. These surprising results can be understood as follows. The energy density is proportional to the local density of electromagnetic states. Close to an interface, there are not only plane waves, which are the solutions of Maxwell equations in a vacuum, but also surface waves. These additional solutions produce a peak of the density of states at a particular frequency, as seen in the dispersion relation of Appendix A. In the case of ionic crystals, the origin of this peak is easy to understand. It is the frequency of the optical phonons which is basically the mechanical eigenfrequency of the atoms in a primitive cell. Since the atoms carry a partial charge, they produce an electromagnetic field. With this picture in mind, it is easy to understand why the density of energy increases when approaching the interface. Each primitive cell is equivalent to an oscillating dipole. As the distance is reduced, the electrostatic contributions in the dipole radiation become the dominating terms.

When comparing the two curves in Fig. 1, it is seen that the effect of the desorder of the amorphous glass is to broaden and to shift the resonance peak. This can be qualitatively understood. Indeed, (i) amorphous glass is a more disordered system so that surface phonon polariton are expected to be strongly damped, and (ii) the local environment of each cell varies from one cell to the other so that a broadening of the spectrum is expected.

B. Spatial coherence

Since we have seen that the electromagnetic field is temporally coherent in the near field, it is natural to revisit its spatial coherence properties. It is also of interest to investigate the role of the structure of the material on the spatial coherence. To this end, we show in Fig. 2 the cross-spectral density of the *z*-component of the electric field along the interface at a distance of $\lambda/20$ for crystalline and amorphous silica. It has been calculated following the procedure outlined in Ref. 1. At a frequency that coincides with the peaks of the density of energy, there are many wave vectors excited so that the spatial spectrum is very broad. Accordingly, the correlation function has a very small range. In contrast, when looking at the cross-spectral density for a lower frequency, we observe a long range correlation of the electromagnetic field along the interface. Similar results were obtained previously for SiC and metals.[1] Not surprisingly, we observe that the coherence length of the amorphous glass is smaller than the coherence length for the crystalline quartz. Yet, it is seen that there exists a non-zero correlation over distances as large as four wavelengths (i.e., 88 μm) for the amorphous glass, indicating that there is still some order on this scale length. The origin of the long-range coherence of a thermal source that support a surface wave can be viewed as follows. The random electric dipole associated with each volume element of the medium excites a surface wave. Since the surface wave is a delocalized mode, the oscillations produced along the surface are coherent within a distance which is given by the decay length of the surface wave. In other words, each volume element is dressed by a surface wave that oscillates coherently over an area determined by the decay length of the surface wave along the interface. Thus each elementary source has an effective spatial extension along

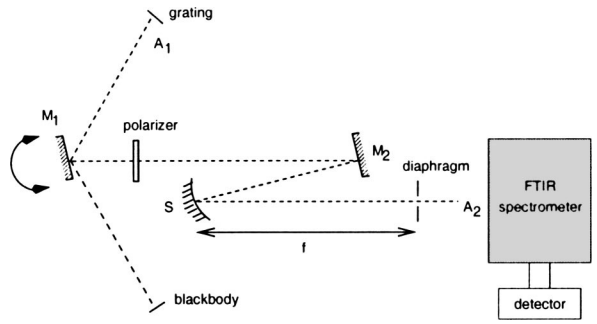

FIG. 3. Experimental setup used for measuring emissivity spectra.

the planar source which may be much larger than the wavelength in vacuum. In what follows, we will use these coherence properties to design sources with specific properties. Depending on the coherence properties, it is possible to design either a highly directional or a quasi isotropic source. In Sec. III, we describe the experimental setup that was built in order to measure the emission with high angular and spectral resolution.

III. EXPERIMENTAL SETUP

A. Optical system

The optical system is schematically shown in Fig. 3. Points A_1 and A_2 are conjugated. A_1 represents the grating or the blackbody and A_2 is the point which is conjugated with the detector through the spectrometer. Thus, the image of the detector determines the area of the sample which is observed. This allows to choose an isothermal area.

A diaphragm (diameter Φ) was placed in the Fourier plane of the spherical mirror. In this position, it makes an angular selection of the directions of emission which are observed. In other terms, we control the solid angle of observation by varying the diameter of the diaphragm. In our setup, $f=300$ mm and $\Phi=3$ mm, so that the solid angle of detection is $\Omega_{\text{detection}}\approx 8\times 10^{-5}$ sr. It is smaller than the solid angle of the natural emission of the grating due to a surface phonon polariton (SPP) $\Omega_{\text{emission}}\approx\pi(\lambda/L)^2$, where $L<1$ mm is the typical propagating length of the SPP on the plane interface. One sees that $\Omega_{\text{emission}}>3.10^{-4}$ sr.

The grating is heated by eight thermal electric resistances and its temperature is controlled by a regulator WEST4200. In the experiment, the target temperature for the grating is 773 K with a precision better than 1 K.

We used an infrared Fourier transform spectrometer DA8 BOMEM. The spectral resolution of this spectrometer varies between 0.01 and 4 cm^{-1}. The measurements have been made with a spectral resolution of 0.5 cm^{-1}, which corresponds to a precision of 5 nm at $\lambda=10$ μm. The detector is a HgCdTe detector cooled at 77 K. Each spectrum is an average of 500 scans: the noise is thus considerably reduced. The beamsplitter of the spectrometer is made of KBr, which is a transparent material in the working frequency range.

B. Experimental procedure

For each angle, we took several measurements of the emission of the sample, of a reference blackbody and of the ambiant radiation. For frequencies below 1500 cm^{-1}, the ambiant radiation reflected on the sample cannot be neglected. The emissivity spectrum S_ε is obtained by subtracting the background signal. The details of the procedure are given in Appendix B.

In order to obtain the emissivity spectrum, we need to know the exact value of the sample temperature. This is achieved by taking advantage of the Christiansen wavelength. At this point, the emissivity ε_λ of the SiC surface is equal to 1. The Christiansen frequency depends neither on the temperature nor on the roughness. We have the following relation:

$$I_{\lambda,T}=\varepsilon_\lambda I^0_{\lambda,T}, \tag{1}$$

where $I_{\lambda,T}$ is the specific intensity of the radiation emitted by the surface at wavelength λ and temperature T, and $I^0_{\lambda,T}$ is the blackbody specific intensity in the same conditions. At the wavelength λ, we can define a temperature T_λ such that $I_{\lambda,T}=I^0_{\lambda,T_\lambda}$. When $\varepsilon_\lambda=1$, we have

$$I_{\lambda,T}=I^0_{\lambda,T}=I^0_{\lambda,T_\lambda}, \tag{2}$$

i.e., $T=T_\lambda$. We can thus determine the exact temperature of the sample. For SiC $\lambda_{\text{Christiansen}}=10.034$ μm. We found that the temperature of the sample in our experiment was $T_S=770$ K.

IV. A QUASIMONOCHROMATIC AND ISOTROPIC THERMAL SOURCE

In this section, we show how to enhance the emissivity of the sample in all directions by taking advantage of the thermal excitation of the surface wave. To this end, we rule a grating on the surface so that the surface wave can be coupled to propagating waves. In order to be able to couple light to any direction, it is necessary to work at a frequency where the dispersion relation is flat (see Appendix A). For fabrication reasons, it is easier to work with a lamellar grating (i.e., with a rectangular surface profile). The characteristics of such a grating are the period Λ, the filling factor F, and the depth h. We optimized the grating parameters in order to maximise the emissivity using a rigorous coupled wave algorithm.[27] For SiC, we found the following characteristics: $\Lambda=3$ μm, $F=0.4$, and $h=0.35$ μm.

In Fig. 4(a), we show two experimental curves, obtained in the conditions described in Sec. III. We represent emissivity spectra for the grating and for the plane interface in p polarization in the normal direction of observation. One can see that a peak appears in the presence of a grating. This peak does not exist for s polarization [see Fig. 4(b)]. The polarization dependence suggests that the grating is not essential but serves to reveal an intrinsic property of the surface. It indicates the role of the SPP in this phenomenon since the SPP exists only for p polarization as discussed in

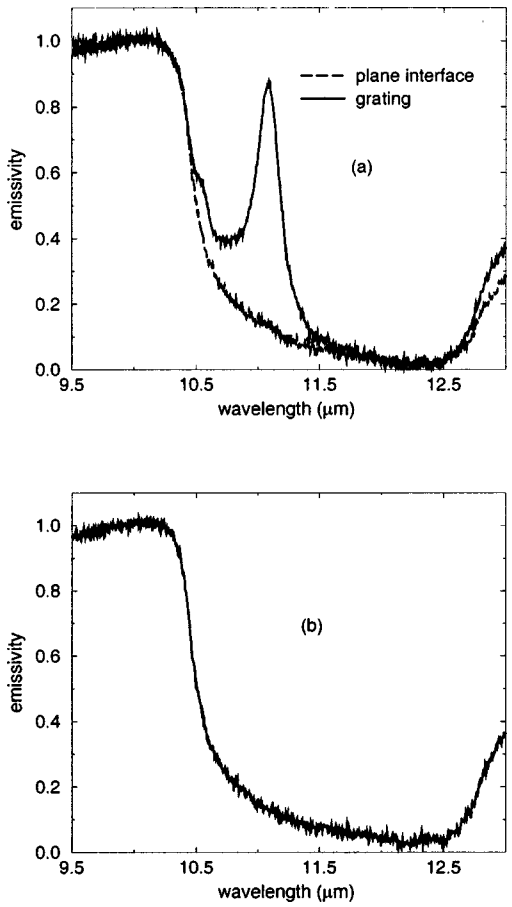

FIG. 4. Emissivity spectra of a smooth grating $\Lambda = 3.00\ \mu$m, $F = 0.4$, and $h = 0.35$. (a) Case of p polarization. (b) Case of s polarization.

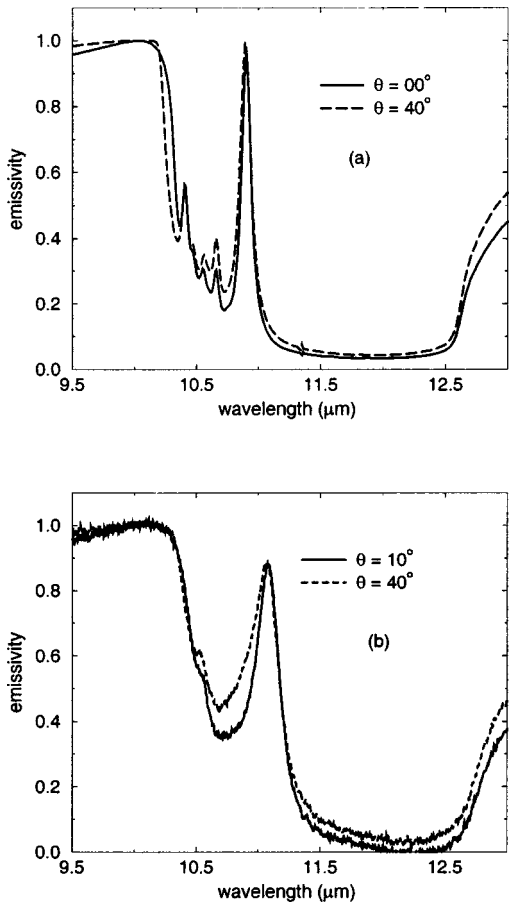

FIG. 5. Emissivity spectra in the p polarization of a smooth grating; $\Lambda = 3.00\ \mu$m, $F = 0.4$, and $h = 0.35$ for two direction of observation $\theta = 10°$ and 40°. (a) Theoretical spectra. (b) Experimental spectra.

Appendix A. Further evidence of the role of the SPP will be given in Sec. V.

When the angle of observation changes, one can see in Fig. 5 that a peak still exists at the same wavelength. Figure 5(a) presents the theoretical spectra and Fig. 5(b) the experimental one. The experimental peak is lower and wider than the theoretical peak. It is also seen that the experimental peak appears at a wavelength $\lambda \approx 11.1\ \mu$m, instead of 10.9 μm in the calculation. We will explain this spectral shift and the broadening of the peak in the following sections.

In Fig. 6, we plot the emissivity versus the angle θ at a fixed wavelength $\lambda = 11.09\ \mu$m. We see that the emission at this wavelength is almost isotropic and increases from a value lower than 0.1 to a value larger than 0.8 at any angle. One can understand this phenomenon by inspection of the dispersion relation (see Appendix A). As a matter of fact the excited SPP lies on the asymptotic branch, characterized by $\omega = 946\ \text{cm}^{-1}$ in the calculation. For a fixed wavelength, there are many SPPs with different wave vectors, i.e., different directions θ of emission. For all these directions the grating emits a quasimonochromatic radiation. Thus, using a SPP thermal excitation, we have succeeded in designing a thermal source which is both isotropic and quasimonochromatic. This concept can be extended to different materials. Tungsten, for instance, is a very good emitter in the visible but its emissivity in the infrared is low. The mechanism that we have described could be used to enhance its emissivity in the infrared, taking advantage of the surface plasmon polaritons.

V. A DIRECTIONAL THERMAL SOURCE

In this section, we consider a grating designed to emit light at a well-defined angle. In order to illustrate the role of the surface wave, we have calculated the emissivity as a function of angle of emission and frequency for a grating. This grating was designed to have a maximum absorption for

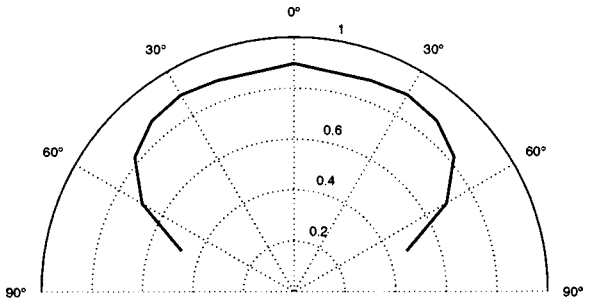

FIG. 6. Experimental emissivity diagram in polar coordinates of a smooth grating; $\Lambda = 3.00\ \mu$m, $F = 0.4$, and $h = 0.35$

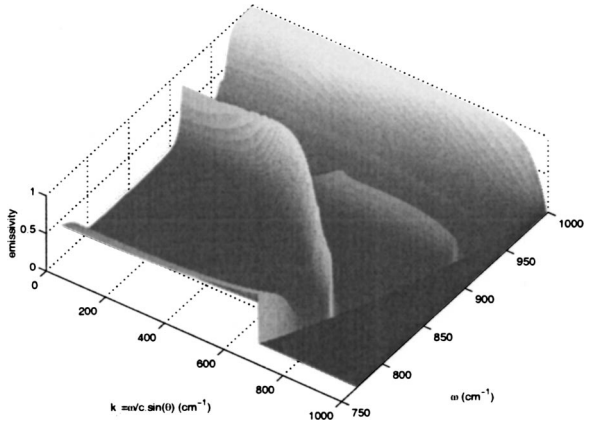

FIG. 7. Emissivity of a SiC grating as a function of frequency and angle of emission. It is seen that the peaks of emission coincide with the dispersion relation of the SPP in the (ω,k) plane.

11.36 μm. The result is displayed in Fig. 7. It is seen that the peaks of emissivity closely follow the dispersion relation of the SPP on a flat surface shown in Fig. 16. In this calculation, we see that the emissivity takes large values for any angle at a particular frequency on the order of 946 cm^{-1}, as already discussed. Furthermore, we see that for lower values of the frequency, the dispersion relation is no longer flat, so that for a given frequency, emission takes place for a well-defined angle. In this part of the spectrum, we expect an angle-dependent spectrum. In other terms, in each direction the grating emits at a different wavelength. We optimized the following characteristics for the grating: $\Lambda = 6.25$ μm, $F = 0.5$, and $h = 0.285$ μm. Such a grating was already studied by Greffet *et al.*[4] In this work we report measurements of the emission spectrum and a quantitative analysis of the data. We will show that we can deduce the coherence length of the source from the emission data. We will also show that it is possible to obtain a quantitative agreement of measurement with theory at high temperature.

We plot the measured emissivity versus the angle θ in Fig. 8 for $\lambda = 11.36$ and 11.89 μm. It is seen that the emission at a fixed wavelength is very directional: the heated grating behaves like an infrared antenna. This is a signature of the spatial coherence of the source. In previously reported measurements, the angular resolution was limited by our signal to noise ratio. We had to increase the aperture of the detection system. The spectral resolution was also limited by signal to noise ratio. In this measurement, we are no longer limited by the instrument in our measurement of the angular width. For instance, our measurement shows that the peaks are narrower when the angle θ increases as predicted by the theory. This will be fully discussed in the following section.

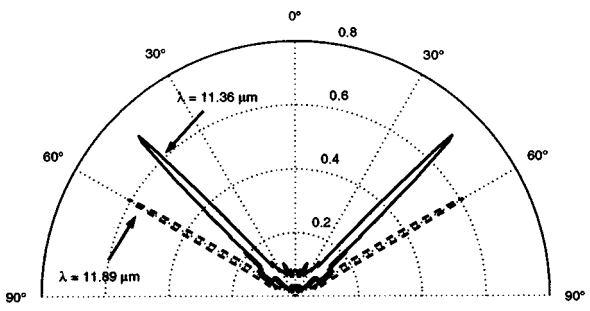

FIG. 8. Experimental emissivity diagram in polar coordinates of a smooth grating; $\Lambda = 6.25$ μm, $F = 0.5$, and $h = 0.285$ at two different wavelengths $\lambda = 11.36$ and 11.89 μm.

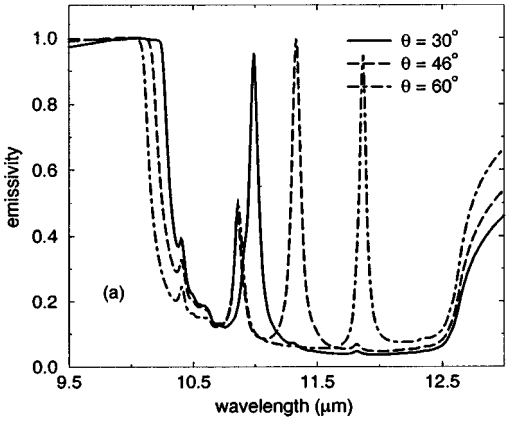

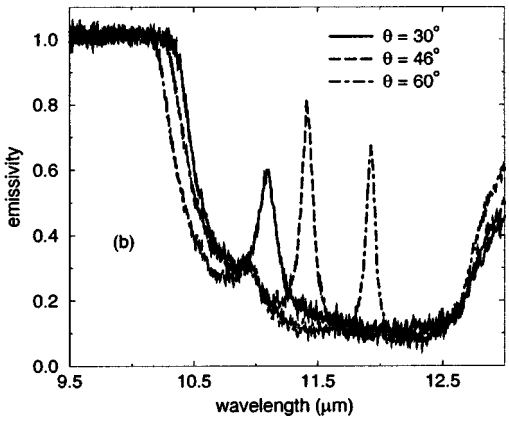

FIG. 9. Emissivity spectra in the p polarization of a smooth grating, $\Lambda = 6.25$ μm, $F = 0.5$, and $h = 0.285$ for three directions of observation $\theta = 30°$, 46°, and 60°. (a) Theoretical spectra. (b) Experimental spectra. The theoretical curve was calculated with the dielectric data at $T = 300$ K, and a grating period of $\Lambda = 6.28$ μm.

We now show the comparison between three theoretical and experimental spectra in Figs. 9(a) and 9(b), respectively, for the angles $\theta = 30°$, 46°, and 60°. As we have seen in Sec. IV, the experimental emissivity is not equal to 1 at the peak wavelength and the peak wavelength is shifted by about 0.1 μm. As in Sec. IV, the experimental peak is wider than the theoretical one. However, the agreement between theory and experiment for reflectivity is excellent as shown in Ref. 4. Thus, we find that theory agrees with reflectivity data but not with emissivity data.

We are now going to analyze the origin of this discrepancy. A possible mechanism is that the grating period varies with the temperature T due to the thermal expansion of SiC as its temperature increases. We measured the period of the grating at 300 and 770 K using a diffraction method. We obtained $\Lambda = 6.26$ and 6.28 μm, respectively, with a precision better than 1%. This variation does not affect signifi-

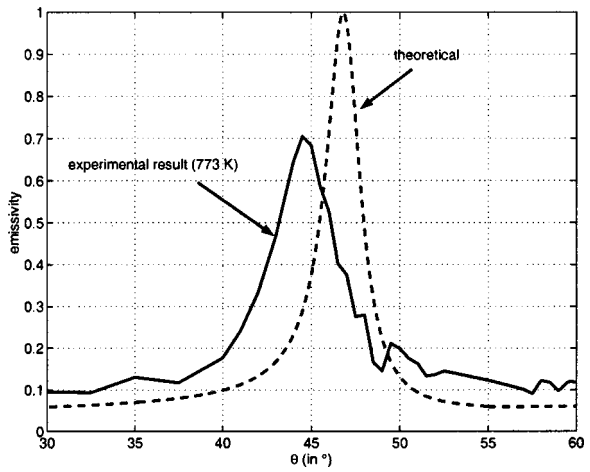

FIG. 10. Experimental emissivity vs the direction of observation θ ($\lambda = 11.36\ \mu$m).

cantly the position of the peak. In Fig. 10 we show the theoretical and experimental emissivity versus the angle of observation θ for a SiC grating with a period $\Lambda = 6.28\ \mu$m at $\lambda = 11.36\ \mu$m. One can see that the thermal expansion of the grating does not explain the experimental result.

Another possible mechanism is the variation of the optical index with temperature. The position of the peak is mainly related to the dependence of the real part ϵ' of the dielectric constant with the temperature T; the width and the height are related to the material absorption, i.e., to the imaginary part ϵ''.

In order to find the dielectric constant at high temperature, we measured the emissivity of a flat surface at normal incidence. We then used a model for the dielectric constant with adjustable parameters. This calculation was made using a Lorentz model by varying ϵ_∞, ω_L, ω_T, and Γ so as to minimize the difference between theoretical and experimental emissivity ε (or reflectivity) as a function of ω. This is achieved by minimizing the following quantity:[28]

$$S = \sum_{i=1}^{N} [\varepsilon_{\exp}(\omega_i) - \varepsilon_{\text{th}}(\omega_i)]^2, \tag{3}$$

where N is the number of experimental points. The number of experimental points was $N = 59$, taken between $\lambda = 9$ and 13 μm. We obtained $\epsilon_\infty = 6.8$, $\omega_L = 959\ \text{cm}^{-1}$, $\omega_T = 779\ \text{cm}^{-1}$, and $\Gamma = 11.7\ \text{cm}^{-1}$. One can see that the variations are not very important (lower than 2%) except for Γ, which has been multiplied by about 2.5. This is not surprising. The main source of losses is phonon scattering. It obviously increases with T. Here we retrieve the increase of the absorption, which can explain the width and the height of the experimental peak.

Finally, we have used the new values of the oscillators parameters ϵ_∞, ω_L, ω_T, and Γ to derive the emission spectrum. In Fig. 11 we show the experimental spectrum at $\theta = 46°$ with the theoretical spectra at both ambiant and high temperature. It is seen that there is a very good agreement between the experiment and the calculation when the proper optical data are used. This confirms that the results depends

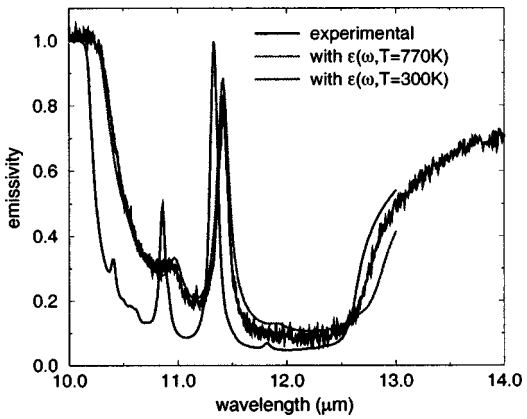

FIG. 11. Experimental and theoretical emissivity spectra. Calculations have been made with two different dielectric constants $\epsilon(\omega)$ at temperatures $T = 300$ and 770 K.

on T through the parameter Γ. We made experiments at different temperatures between 450 and 770 K. In Fig. 12 we show the dependence of the coefficient Γ with the temperature in this range.

VI. MEASUREMENT OF THE COHERENCE LENGTH

We have seen in Sec. V that thermal emission by a SiC grating may become very directional at certain wavelengths. This can be interpreted in terms of spatial coherence: when a source is spatially coherent the radiation emitted by two different points of the source can interfere constructively in a given direction and destructively in the others producing angular lobes. The goal of this section is to use the far field data to recover the coherence length of the field in a plane placed just above the planar source.

We are interested here in the p-polarized emissivity, and the plane of detection is perpendicular to the grating lines. Thus the problem can be fully treated in terms of the scalar magnetic field at a given wavelength $\mathbf{H}(\mathbf{r},\lambda) = H_y(\mathbf{r},\lambda)\mathbf{e}_y$. In this case, we can characterize the spatial coherence with a coherence length calculated via the scalar cross-spectral den-

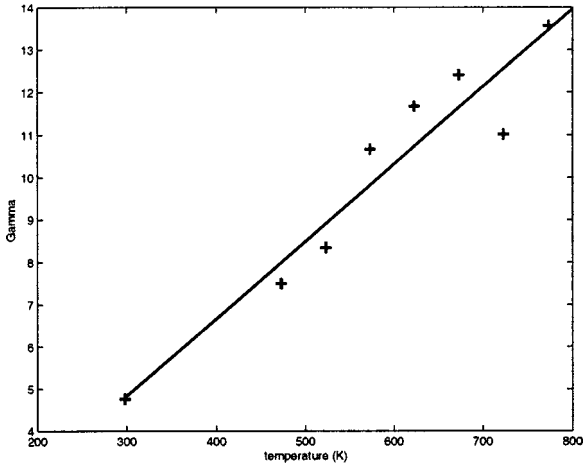

FIG. 12. Variation of the coefficient Γ in the dielectric constant with the temperature.

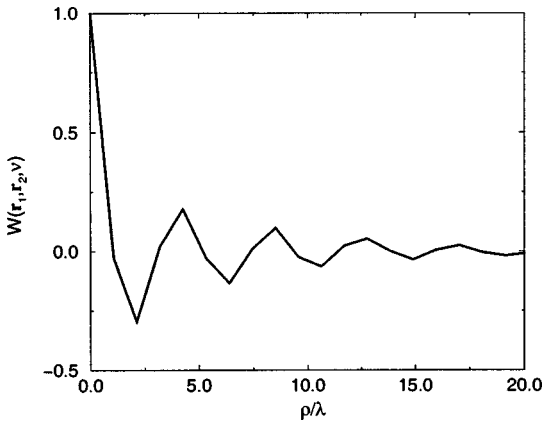

FIG. 13. Spectral degree of spatial coherence for a SiC grating; $\Lambda = 6.25\ \mu$m, $F = 0.5$, and $h = 0.285$ heated at $T = 300$ K.

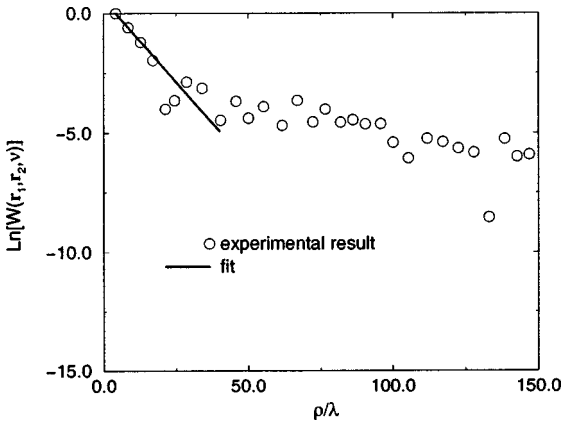

FIG. 14. Determination of the spatial coherence length.

sity function in the near-field $W(\mathbf{r}_1,\mathbf{r}_2,\lambda)$ defined by $W(\mathbf{r}_1,\mathbf{r}_2,\lambda)\,\delta(\lambda-\lambda') = \langle \widetilde{H_y}^*(\mathbf{r}_1,\lambda)\widetilde{H_y}(\mathbf{r}_2,\lambda')\rangle$ where $\widetilde{H_y}$ is the spectral Fourier transform of H_y.[29]

The emissivity diagram yields the radiant intensity in the far-field $J(\mathbf{s},\lambda)$, where $\mathbf{s}=\mathbf{k}/k$ and $\mathbf{k}$ is the wave vector of the incident wave on the detector. It can be shown that[29]

$$W(\mathbf{r}_1,\mathbf{r}_2,\lambda) \propto \int J(\mathbf{s},\lambda)\exp\left(i2\pi\mathbf{s}\cdot\frac{\mathbf{r}_2-\mathbf{r}_1}{\lambda}\right)d^3\mathbf{s}. \qquad (4)$$

$W(\mathbf{r}_1,\mathbf{r}_2,\lambda)$ appears as a spatial Fourier transform of $J(\mathbf{s},\lambda)$ with respect to the variable $(\mathbf{r}_2-\mathbf{r}_1)\lambda$. One must take care that the radiant intensity is defined in the far-field so that we only have access to part of the spectrum of the cross-spectral density. More precisely, the field near the grating at a given wavelength can be split into four contributions:

$$\mathbf{H} = \mathbf{H}_{n-f} + \mathbf{H}_{sw-nr} + \mathbf{H}_{sw-r} + \mathbf{H}_{pw}, \qquad (5)$$

where $\mathbf{H}_{n-f}$ is the very near-field (quasistatic) component of $\mathbf{H}$, $\mathbf{H}_{sw-nr}$ is the field associated with the part of the SPP which is not radiated (part of the dispersion relation lying below the light cone), $\mathbf{H}_{sw-r}$ is the field associated to the part of the SPP which is radiated by the grating and $\mathbf{H}_{pw}$ is the propagating wave contribution. The latter is the only contribution that is emitted in the far field by a flat surface. Only the last two components contribute to the signal received by the detector. These contributions are decorrelated and the cross-spectral density function can be splitted into four parts which are associated with the quasistatic near field, the radiative and nonradiative SPPs, and the natural emission of the sample. The cross-spectral density function reconstructed from the far-field data is thus $W_{\text{calculated}} = W_{sw-r} + W_{pw}$. Note that a flat surface would yield essentially W_{pw}.

In Fig. 13 we plot the reconstructed cross-spectral density function at the wavelength $\lambda = 11.36\ \mu$m versus the quantity ρ/λ, where $\rho = |\mathbf{r}_2-\mathbf{r}_1|$. As discussed above, it contains all the information on the radiated surface wave. This function is normalized by its value at $\rho = 0$. Note that this normalization amounts to plotting the spectral degree of spatial coherence. One can see that the SPP is correlated in the near field over distances ρ of the order of several wavelengths. It is possible to show that the cross-spectral density function decreases exponentially. We define the coherence length as the value of ρ when the spectral degree of coherence is divided by e. In Fig. 14 we plot the neperian logarithm of the envelope of the last curve: it is clearly seen that there is a linear decay between $\rho = \lambda$ and 20λ. The slope yields the coherence length: we obtain on this particular case $L_{\text{coherence}} \approx 7\lambda$. To our knowledge, this is the first measurement of the coherence length of a thermal source. We made the same analysis for the grating at $T = 300$ K, using numerical simulations for the emissivity data. We obtained $L_{\text{coherence}} \approx 11\lambda$. Another calculation was made in Ref. 1 for a plane interface of SiC, where the coherence length at $\lambda = 11.36\ \mu$m was 36λ. We see that the presence of the grating reduces the coherence length by a factor of 3 approximately because of the introduction of radiative losses. Another mechanism that reduces the coherence length is the increase of the damping of the surface phonon polariton due to the increase of the term Γ of the dielectric constant, as seen in Sec. V. This is due to the increase of the phonon-phonon collision as the temperature is increased.

VII. CONCLUSION

In this paper, the coherence properties of thermal near fields have been reviewed. The modification of the coherence properties of the electromagnetic field can be attributed to the presence of surface waves. We have discussed the influence of the microstructure of the material on the temporal and spatial coherence properties. We have shown how the near-field properties can be used to engineer the emission and absorption properties of surfaces. Taking advantage of the flat dispersion relation of the surface wave in a given spectral range, it is possible to produce a source of high emissivity which is almost isotropic and quasimonochromatic. In contrast, when working in the region where the coherence length is large, it is possible to realize a very directional source of light that behaves as an infrared antenna with well-defined lobes. Experimental and theoretical results have been reported showing an agreement better than 2% when proper temperature optical dependent data are used.

From these measurements, we were able to obtain a quantitative value of the coherence length of the thermal sources. This study has highlighted the role of surface waves in the process of light emission by thermal sources. A simple mechanism can be proposed: the first step is excitation of surface waves by thermally excited random dipoles, the second step is the diffraction of the surface waves by a grating. This analysis can have a large impact on the design of light sources. Indeed, the mechanism and the same concepts can be applied to design novel light sources using any physical process that excite surface waves. An advantage of this type of light source is the possibility of engineering the dispersion relation by modifying the surface profile. This allows one to produce either directional or isotropic sources. It also allows one to shift the emission frequency. Finally, we stress that the modification of the dispersion relation amounts to modify the local density of electromagnetic states and therefore, to modify the radiative decay of any type of excitation.

ACKNOWLEDGMENTS

We acknowledge support from Ministere de la recherche, contract Action Concertee Incitative Nanostructures N76-01.

APPENDIX A: SURFACE PHONON POLARITONS ON A PLANE INTERFACE

1. Surface waves at an air/material interface

In this appendix, we briefly review some characteristics of the surface waves which may propagate on a flat material/air interface. A surface wave has an exponential decay away from the interface and propagates along the interface. It is thus a wave that has the forms

$$z>0, \quad \mathbf{E}(x,z)=\mathbf{E}_0 \exp[i(k_{\|}x+\gamma_1 z)], \tag{A1}$$

$$z<0, \quad \mathbf{E}(x,z)=\mathbf{E}_0 \exp[i(k_{\|}x-\gamma_2 z)]. \tag{A2}$$

It can be shown[30,31] that such a solution exists at a vacuum/material interface for materials that have a dielectric constant whose real part is smaller than -1. This happens when the material structure has a resonant behavior. For metals, it corresponds to the plasma oscillation which is a collective oscillation of the electrons.[30,31] For dielectrics, it occurs for frequencies that are in the range of the optical phonons. In both cases, the excitations are delocalized damped modes.

The surface electromagnetic waves are actually charge density waves. Surface plasmon polaritons are due to an acoustic type of oscillation of the electron gas. This mechanical wave of charged particles generates an electric field. The term polariton means that the wave is half an acoustic vibration and half an electromagnetic vibration. In the case of polar dielectrics, the surface waves are called surface phonon polaritons. The underlying microscopic origin is a mechanical vibration of the atoms or phonon. If the phonon takes place in a medium where the atoms carry a partial charge (polar material), the mechanical oscillation is associated with an electromagnetic vibration. Thus, roughly speaking, the surface phonon polariton is half a phonon and half a photon. More precisely, the ratio of mechanical energy to the electromagnetic energy changes continuously as the frequency varies. The horizontal part of the dispersion relation is the phononlike part. In the case of SiC, surface waves are surface phonon polaritons. Other polar materials such as oxydes (e.g. SiO_2) or II-VI and III-V semiconductors for example can also support SPP's. An important property to keep in mind is that surface waves are modes of the interface. Therefore, they can be excited resonantly. It is also important to note that these waves exist only for p polarization, namely for electric fields in the plane (x,z).

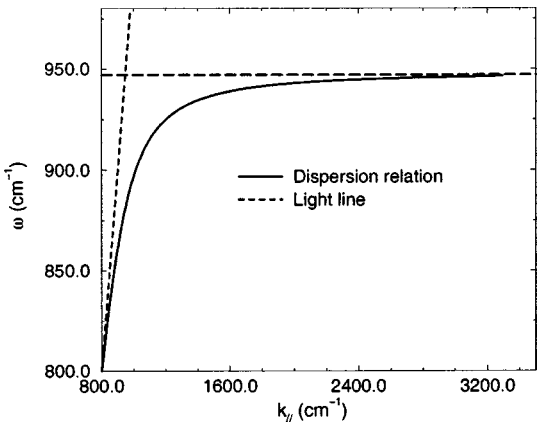

FIG. 15. Dispersion relation of a surface-phonon polariton on a plane surface.

In this paper, we study in detail silicon carbide. This material has interesting properties in the infrared range. Besides, its optical properties $\epsilon(\omega)$ can be described by a simple Lorentz model[28]

$$\epsilon(\omega)=\epsilon_\infty\left[1+\frac{\omega_L^2-\omega_T^2}{\omega_T^2-\omega^2+i\Gamma\omega}\right], \tag{A3}$$

where $\epsilon_\infty=6.7$, $\omega_L=969\ \mathrm{cm}^{-1}$, $\omega_T=793\ \mathrm{cm}^{-1}$, and $\Gamma=4.76\ \mathrm{cm}^{-1}$. The dispersion relation of the SPP has the following dispersion relation for a flat air/material interface:[25,31]

$$k_{\|}=\frac{\omega}{c}\left(\frac{\epsilon(\omega)}{\epsilon(\omega)+1}\right)^{1/2}, \tag{A4}$$

where $k_{\|}$ is the wave vector of the surface mode.

Solving this equation is not trivial. Indeed, $\epsilon(\omega)$ is complex, so in a general case $k_{\|}$ and ω are also complex. Although at first glance, the general choice is to have both quantities complex, it turns out that this is of no use for most cases. The possible choices are either real $k_{\|}$ and complex ω or vice versa. One can show[25] that, for this type of measurement, the dispersion relation is well described by assuming that the wave vector is real and the frequency is complex. In Fig. 15 we plot the dispersion relation for $793<\mathrm{Re}(\omega)<947\ \mathrm{cm}^{-1}$ which corresponds to $\mathrm{Re}[\epsilon(\omega)]<-1$. It is seen that there are two different domains: on the one hand, a linear branch $k_{\|}\approx\omega/c$, and on the other hand an asymptotic branch for $\omega\approx947\ \mathrm{cm}^{-1}$ which corresponds to $\epsilon(\omega)\approx-1$.

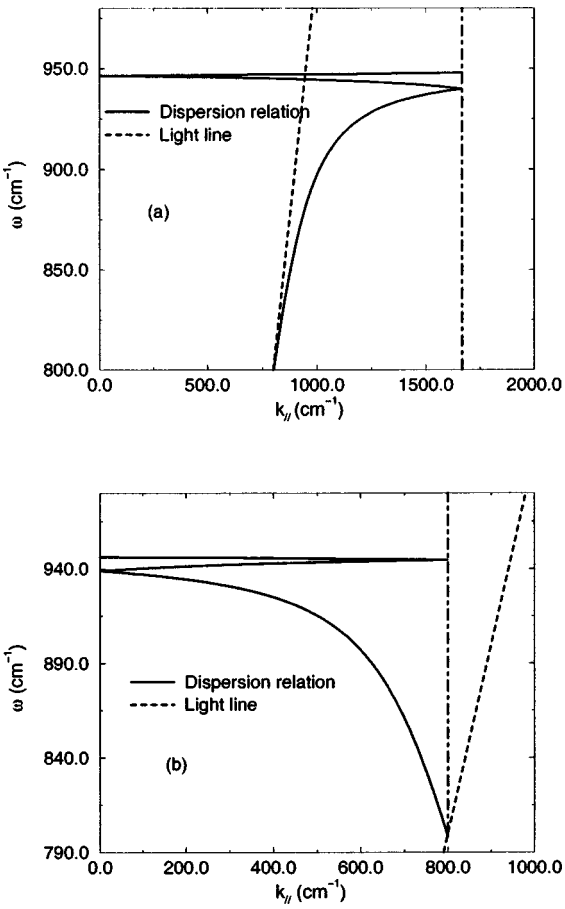

FIG. 16. Dispersion relation of a surface-phonon polariton on a smooth grating. (a) Period $\Lambda = 3.00\ \mu$m. (b) Period $\Lambda = 6.25\ \mu$m.

The curve is under the light line represented by $k = \omega/c$. This means that the solutions are evanescent waves.

2. Role of a smooth grating

As we have seen, the surface wave lies below the light line. All the propagating waves lie above the light line. Since the continuity conditions at the interface demand the frequency and the parallel wave vector to be equal, there cannot be excitation of a surface wave by a propagating plane wave. A well known solution to couple a propagating wave with a SPP is to use a periodic surface. The modes are then Bloch modes whose wave vector is given by

$$\frac{\omega}{c}\sin\theta = k_{\parallel} + m\frac{2\pi}{\Lambda}, \tag{A5}$$

where θ is the angle of propagation, Λ is the grating period and m is the diffraction order. The coupling of an incident propagating wave with a surface mode through the grating can produce up to total absorption.[12] The reciprocal situation is also possible. If a given grating can couple very efficiently the incident light into a surface wave, it can also couple efficiently a surface wave into a propagating mode. This can be used to emit light efficiently. This is the basic mechanism used to produce efficient and coherent thermal sources.

One can interpret Eq. (A5) in terms of dispersion relation. Here we consider that the grating is a smooth perturbation of the flat interface: relation (A4) is still valid. Nevertheless, the dispersion relation can be plotted in a reduced-zone scheme, limited by zero and π/Λ. This reduced-zone scheme depends on the period of the grating. We plot this relation for two different periods $\Lambda = 3$ and 6.25 μm in Figs. 16(a) and 16(b), respectively. It is seen that some parts of the dispersion relation lie in the light cone. These parts are leaky modes ($k_{\parallel} = \omega/c\ \sin\theta, \omega$) which are radiated in the direction θ.

In the first case [Fig. 16(a)], the upper asymptotic branch lies in the light cone. For each $k_{\parallel}$, only one frequency is possible $\omega \approx 947\ \mathrm{cm}^{-1}$. We can expect an emission at a single wavelength in each direction. In the second case [Fig. 16(b)], for a greater period, the linear branch of the dispersion relation lies in the light cone. We can expect a very directional emission at each frequency between $\omega = 793$ and 947 cm^{-1}.

Here we retrieve a feature of the Wolf effect:[32,33] the spectral content is linked to the direction of observation. The observed phenomenon is not only a diffractive effect, but an effect due to the strong spatial and temporal correlation of the SPP.

APPENDIX B: EXPERIMENTAL EMISSIVITY SPECTRUM

In this appendix, we describe the procedure used to obtain the emissivity spectrum from the emission measurements. We denote $S_S^{\mathrm{expt}}(\lambda, T_S)$ the experimental spectrum of the sample at temperature T_S. It can be cast in the form[34]

$$S_S^{\mathrm{expt}}(\lambda, T_S) = R(\lambda)[\varepsilon(\lambda)P(\lambda, T_S) + B(\lambda) + \rho(\lambda)P(\lambda, T_R)], \tag{B1}$$

where $R(\lambda)$ is the instrument response function, $\varepsilon(\lambda)$ the directional emissivity, $P(\lambda, T_S)$ the Planck function at the temperature T_S, $B(\lambda)$ the background radiation reaching the detector directly, and $\rho(\lambda)P(\lambda, T_R)$ the ambiant radiation at the temperature T_R reflected by the sample. $\rho(\lambda) = 1 - \varepsilon(\lambda)$ is the directional reflectivity. Using this relation, we can write

$$S_S^{\mathrm{expt}}(\lambda, T_S) = R(\lambda)\{\varepsilon(\lambda)[P(\lambda, T_S) - P(\lambda, T_R)] + B(\lambda) + P(\lambda, T_R)\}. \tag{B2}$$

When we remove the sample, we measure the spectrum of the room radiation denoted $S_R^{\mathrm{expt}}(\lambda, T_R)$. Eq. (B2) becomes

$$S_R^{\mathrm{expt}}(\lambda, T_R) = R(\lambda)[B(\lambda) + P(\lambda, T_R)]. \tag{B3}$$

We have

$$S_S^{\mathrm{expt}}(\lambda, T_S) - S_R^{\mathrm{expt}}(\lambda, T_R) = R(\lambda)\varepsilon(\lambda)[P(\lambda, T_S) - P(\lambda, T_R)]. \tag{B4}$$

The same procedure for a blackbody at temperature T_B, yields a signal denoted

$$S_B^{\mathrm{expt}}(\lambda,T_B)-S_R^{\mathrm{expt}}(\lambda,T_R)=R(\lambda)[P(\lambda,T_B)-P(\lambda,T_R)]. \tag{B5}$$

Finally, we can obtain the directional emissivity spectrum

$$\varepsilon(\lambda)=\left[\frac{S_S^{\mathrm{expt}}(\lambda,T_S)-S_R^{\mathrm{expt}}(\lambda,T_R)}{S_B^{\mathrm{expt}}(\lambda,T_B)-S_R^{\mathrm{expt}}(\lambda,T_R)}\right]\left[\frac{P(\lambda,T_B)-P(\lambda,T_R)}{P(\lambda,T_S)-P(\lambda,T_R)}\right]. \tag{B6}$$

[1] R. Carminati and J.-J. Greffet, Phys. Rev. Lett. **82**, 1660 (1999).
[2] A. V. Shchegrov, K. Joulain, R. Carminati, and J.-J. Greffet, Phys. Rev. Lett. **85**, 1548 (2000).
[3] C. Henkel, K. Joulain, R. Carminati, and J. J. Greffet, Opt. Commun. **186**, 57 (2000).
[4] J.-J. Greffet, R. Carminati, K. Joulain, J.-P. Mulet, S. Mainguy, and V. Chen, Nature (London) **416**, 61 (2002).
[5] J.-J. Greffet and M. Nieto-Vesperinas, J. Opt. Soc. Am. A **15**, 2735 (1998).
[6] R. Siegel and J. R. Howell, *Thermal Radiation Heat Transfer* (Hemisphere, Washington, D.C., 1981).
[7] A. K. Lorentz, *The Theory of Electrons* (Teibenr, Leipzig, 1916).
[8] A. Jr Banos, *Dipole Radiation in the Presence of a Conducting Half-Space* (Pergamon, Oxford, 1966).
[9] J. E. Sipe, J. Opt. Soc. Am. B **4**, 481 (1987).
[10] H. B. Callen and T. A. Welton, Phys. Rev. **83**, 34 (1951).
[11] S. M. Rytov, Y. A. Kravtsov, and V. I. Tatarskii, *Principles of Statistical Radiophysics* (Springer-Verlag, Berlin, 1989).
[12] R. Petit, *Electromagnetic Theory of Gratings* (Springer-Verlag, Berlin, 1980).
[13] D. Maystre and M. Hutley, Opt. Commun. **19**, 431 (1976).
[14] M. Kreiter, J. Oster, R. Sambles, S. Herminghaus, S. Mittler-Neher, and W. Knoll, Opt. Commun. **168**, 117 (1999).
[15] G. N. Zhizhin, E. A. Vinogradov, M. A. Moskalova, and V. A. Yakovlev, Appl. Spectrosc. Rev. **18**, 171 (1982).
[16] R. W. Gruhlke, W. R. Holland, and D. G. Hall, Phys. Rev. Lett. **56**, 2838 (1986).
[17] P. Andrew and W. L. Barnes, Phys. Rev. B **64**, 125405 (2001).
[18] H. Rigneault, F. Lemarchand, and A. Sentenac, J. Opt. Soc. Am. A **17**, 1048 (2000).
[19] P. J. Hesketh, J. N. Zemel, and B. Gebhart, Nature (London) **324**, 549 (1986).
[20] P. J. Hesketh, J. N. Zemel, and B. Gebhart, Phys. Rev. B **37**, 10795 (1988).
[21] P. J. Hesketh, J. N. Zemel, and B. Gebhart, Phys. Rev. B **37**, 10803 (1988).
[22] M. Auslender and S. Hava, Infrared Phys. Technol. **36**, 1077 (1995).
[23] M. Auslender, D. Levy, and S. Hava, Appl. Opt. **37**, 369 (1998).
[24] H. Sai, H. Yugami, Y. Akiyama, Y. Kanamori, and K. Hane, J. Opt. Soc. Am. A **18**, 1471 (2001).
[25] J. Le Gall, M. Olivier, and J.-J. Greffet, Phys. Rev. B **55**, 10105 (1997).
[26] S. Y. Lin, J.G. Fleming, D.L. Hetherington, B.K. Smith, R. Biswas, K.M. Ho, M.M. Sigalas, W. Zubrzycki, S.R. Kurtz, and J. Bur, Nature (London) **394**, 6690 (1998).
[27] N. Chateau and J.-P. Hugonin, J. Opt. Soc. Am. A **11**, 1321 (1994).
[28] E. D. Palik, *Handbook of Optical Constants of Solids* (Academic Press, San Diego, 1985).
[29] L. Mandel and E. Wolf, *Optical Coherence and Quantum Optics* (Cambridge University Press, Cambridge, 1995).
[30] C. Kittel, *Introduction to Solid State Physics* (Wiley, New York, 1996).
[31] H. Raether, *Surface Plasmons on Smooth and Rough Surfaces and on Gratings* (Springer-Verlag, Berlin, 1988).
[32] E. Wolf, Nature (London) **326**, 363 (1987).
[33] E. Wolf and D. F. James, Rep. Prog. Phys. **59**, 771 (1996).
[34] P. R. Griffiths and J. A. de Haseth, *Fourier Transform Infrared Spectrometry* (Wiley-Interscience, New York, 1986).